Polymer Chemistry

ROYAL SOCIETY OF CHEMISTRY

PAPER

Published on 01 July 2026

Cite this: *Polym. Chem.*, 2026, **17**, 3189

Influence of aliphatic amine grafting on the barrier properties of TEMPO-CNF films

D. Santandrea, [a,b] C. Sillard,[c] C. Rey,[c] V. Beghetto *[a,d,e] and J. Bras [c]

Received 13th May 2026,
Accepted 23rd June 2026

DOI: 10.1039/d6py00462h

rsc.li/polymers

In response to increasing environmental concerns and the growing demand for sustainable materials, this study presents a new approach for enhancing the functional properties of TEMPO-oxidized cellulose nanofiber (TEMPO-CNF) films through aliphatic amine grafting. Surface amidation was carried out using C4–C16 alkyl amines and 4-(4,6-dimethoxy-1,3,5-triazin-2-yl)-4-methyl-morpholinium chloride (DMTMM) as a coupling agent in water–ethanol mixtures under mild conditions (room temperature and neutral pH), thereby avoiding the use of toxic reagents and complex purification steps. Successful covalent grafting was confirmed by ATR-FTIR, elemental analysis, and X-ray photoelectron spectroscopy (XPS). The functionalised films exhibited substantially improved surface and barrier properties, including higher water contact angles (+61%), reduced moisture and water uptake (up to −98%), enhanced water stability (mass loss reduced from 27% to ~3–5%), and lower water vapor permeability (−63%). These improvements were achieved while maintaining high optical transparency and largely preserving the oxygen barrier properties of the films. Soil burial tests revealed a clear relationship between surface hydrophobicity and biodegradation behaviour. Films modified with short-chain amines underwent complete degradation within a few weeks, whereas those functionalised with longer alkyl chains showed only partial degradation after 24 weeks. Overall, the DMTMM-mediated aqueous amidation strategy provides a simple, environmentally friendly, and effective route for tailoring the surface characteristics of TEMPO-CNF films, expanding their potential for advanced packaging and barrier applications.

Introduction

The widespread use of non-biodegradable, fossil-based materials represents a major source of environmental pollution.[1–3] Recent studies have also highlighted the potential health risks associated with their production, use, and disposal.[4] Among the various application sectors, packaging, for food, beverages, and consumer goods, among others, is one of the largest consumers of plastics, accounting for approximately 40% of global fossil-based plastic production and use. In response to growing environmental and health concerns, increasing efforts have been directed toward the development of sustainable alternatives, particularly bio-based and biodegradable materials for packaging applications.[5–11]

Commonly studied biopolymers include polysaccharides such as cellulose, starch, and chitosan, as well as proteins like gelatin.[12–16] However, despite their renewable origin and biodegradability, these materials often suffer from drawbacks such as high water sensitivity and inadequate barrier properties, which limit their applicability in demanding packaging environments.

Among bio-based polymers, cellulose stands out, due to its natural abundance, biodegradability, and mechanical properties, making it one of the most extensively studied materials in this context.[17–23] Within this panorama, nanostructured cellulose, including cellulose nanofibers (CNFs) and their TEMPO-oxidized form (TEMPO-CNF), has attracted growing interest as a promising alternative to fossil-based plastics.[24] TEMPO-CNF films exhibit high optical transparency, excellent mechanical strength, and good oxygen barrier performance.[25,26] Nevertheless, their high hydrophilicity and poor water resistance remain key challenges, particularly in packaging applications where resistance to moisture and water vapor is essential.

To overcome these limitations, chemical modification has emerged as a promising strategy for enhancing the functional properties of TEMPO-CNF films.[27] In particular, the presence of carboxylate groups on the surface of TEMPO-CNF provides

[a]*Dipartimento di Scienze Molecolari e Nanosistemi, Università Ca' Foscari Venezia, Via Torino 155, 30172 Venezia, Italy. E-mail: beghetto@unive.it*
[b]*Dipartimento di Architettura e Disegno Industriale, Università della Campania "Luigi Vanvitelli", Via San Lorenzo-Abazia di San Lorenzo, 81031-Aversa, CE, Italy*
[c]*Univ. Grenoble Alpes, CNRS, Grenoble INP, LGP2, 461 Rue de la Papeterie, Grenoble, France*
[d]*Crossing S.r.l., Viale della Repubblica 193/b, 31100 Treviso, Italy*
[e]*Consorzio Interuniversitario per le Reattività Chimiche e La Catalisi (CIRCC), Via C. Ulpiani 27, 70126 Bari, Italy*

reactive sites for targeted functionalisation, enabling improvements in water resistance and barrier properties.[5,28]

This study presents a proof of concept for the surface modification of TEMPO-CNF films aimed at improving their water-resistance properties through amidation with aliphatic amines using the water-compatible condensation agent 4-(4,6-dimethoxy-1,3,5-triazin-2-yl)-4-methylmorpholinium chloride (DMTMM). DMTMM is regarded as a more sustainable alternative to conventional coupling systems such as EDC/NHS because of its high efficiency, ease of use and low toxicity.[29–37]

The modification protocol was designed to be simple, efficient and environmentally friendly. TEMPO-CNF films were immersed in a water–ethanol solution containing DMTMM and selected amines at neutral pH, followed by a straightforward purification step. A series of aliphatic amines with different alkyl-chain lengths (C4–C16) were employed to evaluate the versatility of the grafting process and to systematically tailor the surface properties of the resulting films. Importantly, a clear quantitative correlation was established between the experimental diffusion coefficients (D) of the free amines in the reaction medium determined by DOSY and their resulting surface (DSS) and bulk (DS) degrees of substitution, providing a predictive framework for the heterogeneous amidation of nanocellulose.

The modified films were comprehensively characterized using ATR-FTIR, atomic force microscopy (AFM), elemental analysis, UV-vis spectroscopy, and X-ray photoelectron spectroscopy (XPS) to confirm successful surface functionalisation. Functional properties relevant to packaging applications were then evaluated, including surface hydrophobicity (water contact angle and surface energy), interactions with moisture and gas (moisture uptake, water vapor permeability, and oxygen transmission rate), and resistance to water (water uptake, water stability, and water permeability).

Finally, soil-burial biofragmentation tests were performed to assess the effect of chemical modification on the intrinsic biodegradability of TEMPO-CNF films.

Materials and methods

Materials

TEMPO-CNF (degree of oxidation = 1.39 $mmol_{COONa}$ g^{-1}) 1 wt% aqueous suspension was purchased from the University of Maine (USA); butylamine, octylamine, dodecylamine, hexadecylamine, sulfanildiazine and DMTMM were purchased from Merck (St Louis, MO). All reagents were used as received without any further purification.

Methods

Film preparation. TEMPO-CNF films were prepared using a casting method at 30 °C for 48–72 h starting from 30 g of 1 wt% TEMPO-CNF poured into a polystyrene Petri dish with a diameter of 9 cm. Films obtained had a thickness between 30 μm and 40 μm and were used for chemical grafting. *Film grafting.* (1) Amine–DMTMM solution preparation: 1 mmol of amine (73 mg of butylamine, 129 mg of octylamine, 185 mg of dodecylamine, and 241 mg of hexadecylamine) was solubilized in 10 mL of ethanol. An aqueous solution of 0.1 M HCl was added dropwise until pH 7 was reached. The total volume of the solution was adjusted to 20 ml by adding distilled water in order to obtain 0.05 M amine in 1/1 v/v water–ethanol at pH 7. To this solution, 550 mg (2 mmol) of DMTMM was added to achieve 0.1 M concentration. (2) The TEMPO-CNF film (200 mg) was soaked for 20 h at 30 °C in the reactive DMTMM/amine solution. (3) At the end of the reaction, the film was washed five times using ultrasound with a 1/1 v/v water–ethanol solution and left to dry at room temperature. *ATR FT-IR*. Infrared spectra were recorded directly on the TEMPO-CNF films using an ATR-FTIR PerkinElmer 1720X spectrometer in attenuated total reflectance (ATR) mode. The ATR-FTIR spectra were collected with a resolution of 2 cm^{-1} in the range of 4000–600 cm^{-1}. Thus, 16 scans were collected in duplicates. To obtain samples with protonated carboxylic moieties, a film specimen was immersed in aqueous hydrochloric acid at pH 3 for 30 minutes, washed with distilled water and dried at room temperature. *Elemental analysis and degree of substitution*. Elemental analysis (CHN) data were collected using an Unicube organic elemental analyser. Each experiment was performed in duplicate. Sulfanildiazine was employed as the standard. The degree of substitution (DS) was calculated from these data using eqn (1) previously used by Le Gars and coworkers:[38]

$$DS = \frac{\%N \times (M_{AGU} + DO \times (M_{AGU\text{-}COONa} - M_{AGU})}{M(N)_{grafted} - \%N \times M_{grafted}} \quad (1)$$

M_{AGU} and $M_{AGU\text{-}COONa}$ are the total molar mass of AGU (162.14 g mol^{-1}) and the molar mass of oxidized AGU with sodium salt as the counter ion (198.11 g mol^{-1}). The terms % N, $M(N)_{grafted}$, $M_{grafted}$ and DO correspond to the nitrogen content in the modified CNF sample obtained by elemental analysis, the nitrogen molar mass of the grafted moieties (14.0 g mol^{-1}), the total molar mass of the grafted moieties (72.13 g mol^{-1} for C_4-NH_2, 128.24 g mol^{-1} for C_8-NH_2, 184.35 g mol^{-1} for C_{12}-NH_2, 240.46 g mol^{-1} for C_{16}-NH_2), and the degree of oxidation of TEMPO-CNF, found to be 0.67, respectively. The degree of substitution corresponds to the number of amine compounds introduced in each AGU. *XPS measurements.* Surface chemical analysis was conducted using X-ray photoelectron spectroscopy (XPS), with an analysed depth of less than 10 nm. An XPS K-Alpha device (ThermoFisher) was employed. The substrates were positioned at an angle of 90° under an ultrahigh vacuum of less than 10^{-7} Pa. Peak deconvolution analysis was performed using the OriginPro 8.5 software. The applied sensitivity factors were 0.001772 for O, 0.00059 for C, and 0.00109 for N. Each peak area was divided by its respective sensitivity factor to normalize the elemental response and obtain accurate atomic ratios. The surface degree

of substitution (DSS) was calculated using Gousse's equation,[39,40] shown in eqn (2):

$$\mathrm{DSS} = \frac{M_{\mathrm{AGU}} \times \%\mathrm{N}}{100 \times M(\mathrm{N}) - M_{\mathrm{grafted}} \times \%\mathrm{N}} \quad (2)$$

where M_{AGU} is the molecular weight of the anhydroglucose unit (162.14 g mol^{-1}), %N is the concentration of the nitrogen detected by XPS and M_{grafted} is the molecular weight of the grafted moieties. *Coefficient of diffusion.* The diffusion-ordered spectroscopy (DOSY) NMR experiments were performed using a Bruker Avance 600 MHz spectrometer. The data were acquired and processed using TopSpin 4.5.0 software, applying the standard predefined Bruker DOSY processing routine. Experiments were performed by dissolving approximately 30 mg of amine in 0.6 mL of a 1 : 1 (v/v) mixture of deuterium oxide and deuterated ethanol, in order to simulate the reaction environment. The solution was previously neutralized by adding one drop of 35% deuterated hydrochloric acid.

Film thickness. Film thickness measurements were performed using a Lhomargy micrometer (±0.01 mm). At least five measurements were performed for each sample. For each amine used, film specimens prepared *via* at least two different reactions were used and the film thickness was obtained as the average of these values. *UV-vis analysis.* The UV-vis spectroscopy analysis of all films prepared was carried out using an Agilent Cary 100 UV/vis spectrophotometer (Milano, Italy). The films were placed directly into the spectrophotometer test cell, and air was used as the reference. The optical absorbance and transmittance of the films were measured in the wavelength range of 200–800 nm with a scan rate of 600 nm min^{-1}. Transparency measurements were carried out on F0–F16 films by measuring the absorbance at 600 nm and calculated according to eqn (3):[41]

$$\mathrm{Transparency} = (\log T600)/t \quad (3)$$

where $T600$ is the value of transmittance at 600 nm and t is the film thickness (mm). All measurements were performed in triplicate. *Water uptake.* The water uptake of the films was determined according to a method reported in the literature. Film specimens of 2 × 2 cm were immersed in water and at regular intervals were extracted and excess water was gently removed using absorbent paper. Water absorption was calculated according to eqn (4):

$$\mathrm{WU} = \frac{(W_{\mathrm{wet}} - W_{\mathrm{dry}})}{W_{\mathrm{dry}}} \quad (4)$$

where W_{wet} is the weight of the sample immersed in water and W_{dry} is the initial weight of the sample. All experiments were performed in triplicate using film specimens prepared *via* two different reactions. *Water stability.* Film specimens of approximately 20 mg were immersed in 10 mL of water for 24 h. They were extracted and dried at 105 °C. The water stability was calculated according to eqn (5):

$$\mathrm{WS} = \frac{(W_{24} - W_0) \times 100}{W_0} \quad (5)$$

where W_0 is the starting film weight and W_{24} is the dried film weight after 24 h of water immersion. All experiments were performed in triplicate using film specimens prepared *via* at least two different reactions. *Contact angle*. The contact angles of the films with various liquids were measured using a Data Physics OCA device. The contact angle values for the static determination and for surface energy determination were taken after 5 seconds. All experiments were performed in triplicate using film specimens prepared *via* at least two different reactions. *Surface energy.* The surface energy was determined using the Owens–Wendt method. By the linear regression ($y = ax + b$) of the Owens equation, the polar and dispersive components of the solid were calculated according to eqn (6):

$$\gamma_{\mathrm{s}}^{\mathrm{d}} = b^2;\ \gamma_{\mathrm{s}}^{\mathrm{p}} = a^2;\ x = \left(\frac{\gamma_{\mathrm{L}}^{\mathrm{p}}}{\gamma_{\mathrm{L}}^{\mathrm{d}}}\right)^{\frac{1}{2}};\quad y = \gamma_{\mathrm{L}}(1 + \cos(\theta))/\left[2(\gamma_{\mathrm{L}}^{\mathrm{d}})^{\frac{1}{2}}\right] \quad (6)$$

where γ_{L} is the total surface tension of the liquid, $\gamma_{\mathrm{L}}^{\mathrm{p}}$ is the polar component of the liquid surface tension, $\gamma_{\mathrm{L}}^{\mathrm{d}}$ is the dispersive component of the liquid surface tension, θ is the contact angle of the testing liquid, $\gamma_{\mathrm{s}}^{\mathrm{d}}$ is the dispersive component of the solid surface energy and $\gamma_{\mathrm{s}}^{\mathrm{p}}$ is the polar component of the solid surface energy. The total surface energy of the solid surface is given by the sum of polar and dispersive components. Two different liquids were tested for surface energy determination: water ($\gamma_{\mathrm{L}}^{\mathrm{p}}$ = 51.2 mN m^{-1}; $\gamma_{\mathrm{L}}^{\mathrm{d}}$ = 21.8 mN m^{-1}) and diiodomethane ($\gamma_{\mathrm{L}}^{\mathrm{p}}$ = 0 mN m^{-1}; $\gamma_{\mathrm{L}}^{\mathrm{d}}$ = 50.8 mN m^{-1}). *Water vapor transmission rate (WVTR) and water vapor permeability (WVP)*. Cups with an average diameter of 3.5 cm and a volume of 70 mL were used to determine the water vapor transmission rate (WVTR) of the films. Each cup was covered with a film and sealed to the cup using paraffin. Cups containing anhydrous $CaCl_2$ (RH = 0%) were placed in a desiccator with a saturated solution of sodium chloride (RH = 75%) at 25.0 ± 2 °C. Cups were weighed every hour for 8 h and finally after 24 h. The water vapor transmission rate (WVTR) was calculated according to eqn (7):

$$\mathrm{WVTR} = \frac{24X}{AY} \quad (7)$$

where X is the mass gain in grams in the period Y (hours) and A is the exposed area in m^2. All experiments were performed in triplicate using film specimens prepared *via* at least two different reactions. Water vapor permeability (WVP) was measured according to eqn (8):

$$\mathrm{WVP} = \frac{\mathrm{WVTR} \times t}{P(R_1 - R_2)} \quad (8)$$

where t is the film thickness (m) and $P(R_1 - R_2)$ is the driving force term given by water saturation pressure P, relative humidity in the desiccator R_1 (0.75) and relative humidity in the cups R_2 (0). This term is equal to 1753.55 Pa. *Water permeability.*

Water permeability experiments were performed using a self-designed experimental setup. A glass tube with an area of 20 cm^2 was sealed on a TEMPO-CNF film with paraffin oil and the whole system was placed on a filter paper specimen previously dried at 50 °C for 1 h and weighed. Then, 5 mL of deionized water was poured into a glass tube. After 5 minutes, the paper was removed and weighed. Water permeability WP was determined according to eqn (9):

$$\mathrm{WP} = \frac{W_f - W_0}{A} \quad (9)$$

where W_f is the weight in grams of the filter paper after contact with the film, W_0 is the initial weight in grams of the dried filter paper, and A is the contact area (m^2). All measurements were performed in triplicate. *Oxygen permeability (OP).* OP of F0 and C_{4-16}-NH_2 films were measured using a Presens oximeter (Pts3 sensors), following the DIN 53380-5 standard. The measurement was performed using dry oxygen (0% RH). Each sample was cut to fit a 26 mm diameter dish and tested for at least 24 hours. The reported value was determined from the slope of the oxygen uptake as a function of time. OP was measured according to eqn (10):

$$\mathrm{OP} = \frac{Q \times t}{A \times \mathrm{day}} \quad (10)$$

where Q is the total volume of oxygen transmitted (cc), A is the area of the sample (m^2) and t the thickness of the film (m). For measurements below the limit of detection (LOD), a value corresponding to 50% of the LOD (0.01 cc m^{-1} day^{-1}) was assigned for the purpose of data analysis.[42] *Biofragmentation tests.* Biofragmentation tests were carried out according to the G160-12 standard with slight modifications. A 9 cm^2 specimen was introduced into the soil at a depth of approximately 3 cm after being dried at a temperature of 105 °C and weighed. The soil used consisted of equal parts of fertile topsoil, well-rotted and shredded horse manure and coarse sand. The soil was humidified with water at 7 day intervals. The test was carried out in a 50% RH environment at 23 °C. Specimens were taken at regular intervals, gently washed with ethanol and dried at a temperature of 105 °C until constant weight. The relative weight loss caused by biofragmentation was evaluated according to eqn (11):

$$\text{Weight loss } (\%) = ((W_0 - W_t) \times 100)/W_0 \quad (11)$$

where W_0 is the initial weight and W_t is the weight of the sample at a given time. All measurements were performed in triplicate.

Results and discussion

Functionalisation of TEMPO-CNF films

TEMPO-CNF films were obtained using a simple casting procedure from a 1 wt% TEMPO-CNF aqueous suspension as reported in the literature.[43] TEMPO-CNF films were directly amidated by treatment with a water/ethanol solution containing an alkylamine and the activating condensation agent (DMTMM) (Scheme 1). A water/ethanol (1/1 vol/vol) mixture was selected as the solvent for the reaction, since ethanol promotes dissolution of non-polar reagents and ensures stability of the TEMPO-CNF films, which are unstable in pure water, often leading to fiber redispersion. The reactions were performed at neutral pH to promote amine solubility through partial protonation while ensuring efficient activation by DMTMM, which exhibits optimal reactivity in the pH range of 7–9.[44,45]

Different amines (butylamine, octylamine, dodecylamine, and hexadecylamine) were used to generalize the process and explore the tunability of the properties due to surface grafting. Each film was labelled according to the amine used (see Table 1). Ultrasound-assisted washing steps were employed to purify the TEMPO-CNF film surface. Following grafting and washing, the films retained their visual integrity, with no observable damage, pores, or colour change, and only a slight increase in film roughness was observed (2.71 nm for C_4-NH_2; 5.75 nm for C_8-NH_2; 2.01 nm for C_{12}-NH_2; and 3.42 nm for C_{16}-NH_2).[46]

To highlight the essential role of DMTMM-mediated covalent bond formation on surface grafting of TEMPO-CNF films, two preliminary experiments were carried out with and without DMTMM in the presence of butylamine (C_4-NH_2 and C_4-NH_2B, Table 1). ATR FT-IR analysis was performed to characterize the control sample F0 (unmodified TEMPO-CNF), C_4-NH_2, and C_4-NH_2B (Fig. 1a). From these spectra, it evidently appears that F0 and C_4-NH_2B are equivalent, while in the ATR FT-IR spectra of C_4-NH_2, a new signal at 1650 cm^{-1} corresponding to a shift of the carbonylic signal of the amide[31,38] and the aliphatic C–H stretching of the amine (2850 cm^{-1}) were evidenced, confirming the grafting of the amine on the TEMPO-CNF surface.

Since the signal of the unreacted carboxylate functional groups (1600 cm^{-1}) partially overlaps that of the amidic groups (1650 cm^{-1}), the C_4-NH_2 sample was treated with an HCl–water solution at pH 3 to protonate the unreacted carboxylate groups, and ATR-FTIR was repeated (Fig. 1b).

The acid treatment leads to a shift of the –COOH groups to 1720 cm^{-1}, allowing to unambiguously assign the signal of the amidic groups, which remain unchanged at 1650 cm^{-1}. Thus, these preliminary experiments highlight that DMTMM is crucial for achieving the grafting of the amine on TEMPO-CNF.

Based on these findings, TEMPO-CNF was further treated with other amines (C_8-NH_2, C_{12}-NH_2, C_{16}-NH_2, Table 1). The ATR-FTIR spectra of C_8-NH_2, C_{12}-NH_2, and C_{16}-NH_2 TEMPO-CNF films shown in Fig. 1c are equivalent to that of C_4-NH_2, confirming the grafting of TEMPO-CNF films with all amines tested. It is interesting to note that as the alkyl chain length of the amine increased, the intensity of the C–H stretching band at 2850 cm^{-1} assigned to the longer amine chains also increased, and the broad hydroxyl band at 3300 cm^{-1} decreased because of a reduction in moisture uptake.

Elemental analysis allowed us to determine the nitrogen content and calculate the degree of substitution (DS) of the

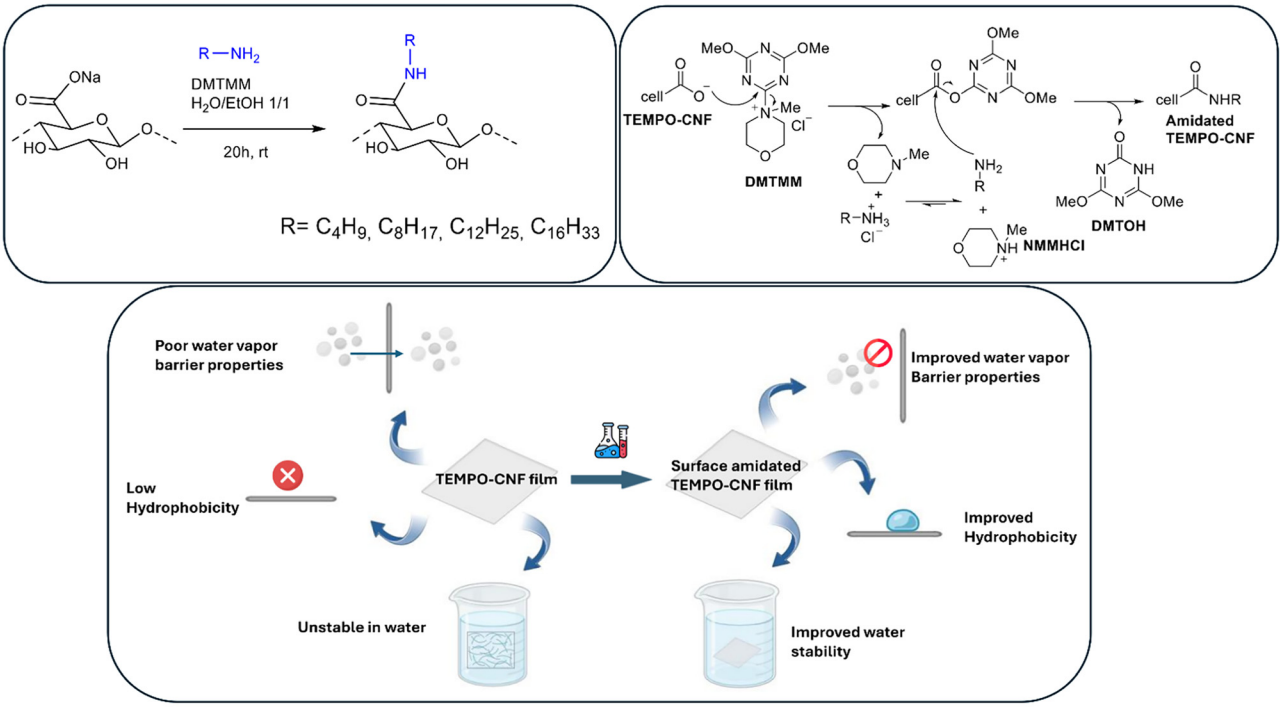

Scheme 1 Amidation of TEMPO-CNF films mediated by DMTMM and potential impact of the grafting on the functional properties.

Table 1 Film labels

Amine[a]	Amine/DMTMM (mol : mol)[b]	Film label
—	—	F0
Butylamine	1 : 2	C_4-NH_2
Butylamine	—	C_4-NH_2B
Octylamine	1 : 2	C_8-NH_2
Dodecylamine	1 : 2	C_{12}-NH_2
Hexadecylamine	1 : 2	C_{16}-NH_2

[a] Amine: 0.05 mmol. [b] DMTMM: 0.1 mmol.

grafted samples (C_4-NH_2, C_8-NH_2, C_{12}-NH_2, and C_{16}-NH_2). The DS, representing the number of amines bonded per anhydroglucose unit in TEMPO-CNF, was calculated to be between 0.10 and 0.12, as shown in Table 2 (see the Materials and methods section).

X-ray photoelectron spectroscopy (XPS) was employed to investigate the surface composition (up to ~10 nm depth) of TEMPO-oxidized cellulose nanofibrils (TEMPO-CNFs) and the grafted films (Fig. 2a). In the grafted TEMPO-CNF samples, a new peak was evidenced around 400 eV (Fig. 2b–e), attributable to the nitrogen of the amine. This peak was deconvoluted into two components at 401.6 eV and 399.6 eV, corresponding to N–C═O (amide bonds) and N–H/N–C bonds, respectively.[47] A peak area ratio of 1 : 2 between the N–C═O and N–H/N–C components is expected if the amines are exclusively retained through covalent amide bonding.[38] This ratio is very close to that registered for the C_4-NH_2-grafted sample (1 : 1.8), suggesting that nitrogen is predominantly present in the amide form. For samples functionalised with longer alkyl chains (Fig. 2c–e), the ratio slightly increases, indicating the potential presence of physically adsorbed amines on the film surface. This could be a consequence of stronger supramolecular interactions between the long alkyl chains and the cellulose surface, which may hinder complete removal of unbound amine during washing.

Further information was obtained from high-resolution C 1s spectra (Fig. 2f–i), with the deconvolution data summarized in Table 3. The unmodified TEMPO-CNF sample exhibited unusually high intensities in the C–C/C–H region, likely due to surface contamination, as lower values are typically reported in the literature.[48] In the grafted samples ($C_{4-16}NH_2$), the carbon peaks were deconvoluted into five distinct components, attributed to C–C/C–H (284.7 eV), C–N (285.3 eV), C–O (286.3 eV), O–C–O (287.8 eV), and O–C═O (289.1 eV), in accordance with previous studies.[38,39,47] The O/C atomic ratio progressively decreases with increasing alkyl chain length, consistent with the incorporation of carbon-rich alkyl chains on the film surface. Similarly, the N/O ratio increases with chain length, primarily due to a relative decrease in surface oxygen concentration.

The surface degree of substitution (DSS), calculated using Gousse's equation, ranged from 0.11 to 0.26. Interestingly, the ratio between DSS and the total degree of substitution (DS) varied significantly depending on the amine used. For butylamine, this ratio was approximately 1.1, suggesting that due to its small molecular size, it diffuses into the bulk of the film during the reaction.

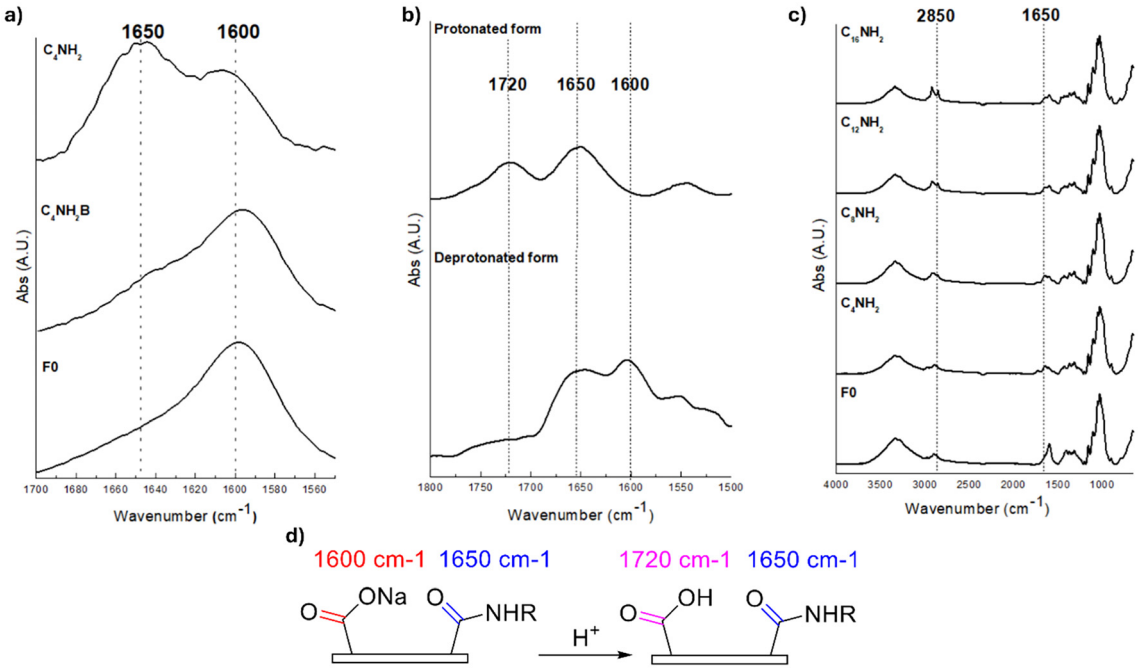

Fig. 1 (a) ATR-FTIR spectra comparison between the starting material F0, blank and C_4-NH_2; (b) ATR-FTIR spectra comparison between protonated and deprotonated C_4-NH_2 samples; (c) ATR-FTIR stacking of functionalised films; and (d) graphical visualization of various carbonyl forms on the TEMPO-CNF surface.

Table 2 Elemental analysis, thickness and roughness data

Film	No. [a]	N_{EA} (%)	C_{EA} (%)	H_{EA} (%)	C/N_{EA} ratio	C/H_{EA} ratio	DS_{EA}	Thickness (μm)	Roughness (R_a) (nm)
F0	—	0.02	38.6	5.2	—	7.3	—	33.8 ± 0.2	1.22
C_4-NH_2	4	0.90	42.1	6.3	44.8	6.7	0.10	31.8 ± 2.5	2.71
C_8-NH_2	8	1.00	44.1	6.5	45.2	6.7	0.12	36.3 ± 1.0	5.75
C_{12}-NH_2	12	1.00	46.0	6.9	46.7	6.6	0.12	39.8 ± 1.2	2.01
C_{16}-NH_2	16	1.20	49.9	7.5	42.7	6.6	0.11	46.2 ± 2.5	3.42

[a] No.: number of carbon atoms present in the amine.

In contrast, longer-chain amines (octylamine, dodecylamine, and hexadecylamine) exhibited significantly higher DSS/DS ratios, indicating that these bulkier molecules remain predominantly on the surface, as their larger molecular volume limits diffusion into the film. This phenomenon was further confirmed by measuring the diffusion coefficients (D) of the free amines in the aqueous reaction medium *via* DOSY-NMR experiments. The progressive decrease in the diffusion coefficient observed with increasing alkyl chain length provides strong quantitative evidence of the growing resistance to molecular migration within the swollen TEMPO-CNF network. Consequently, longer-chain species are restricted to reacting almost exclusively at the film interface (Table 4). To the best of our knowledge, this approach directly correlates the solution-state diffusivity of the modifiers with their surface-*versus*-bulk reactivity trends for the first time. This mechanistic insight establishes a critical benchmark for predicting and controlling the heterogeneous functionalisation of TEMPO-CNF films in aqueous media.

Characterization of TEMPO-CNF film structure and transparency

DMTMM-mediated amidation allowed us to perform the reaction at room temperature, preventing an increase in yellowness of the material (Fig. 3a), typically observed in TEMPO-CNF films when the process is carried out at higher temperatures.[49] Optical properties were analysed using UV-vis spectroscopy, with the absorbance and transmittance spectra shown in Fig. 3b and c. As the alkyl chain length of the amine increased, a slight reduction in transparency was measured. These observations are supported by transparency measurements shown in Fig. 3d, following the method of Han and Floros.[41] AFM analysis of TEMPO-CNF fibers (Fig. 3e) used for film production showed an average diameter of the fibers of 24 ± 4 nm

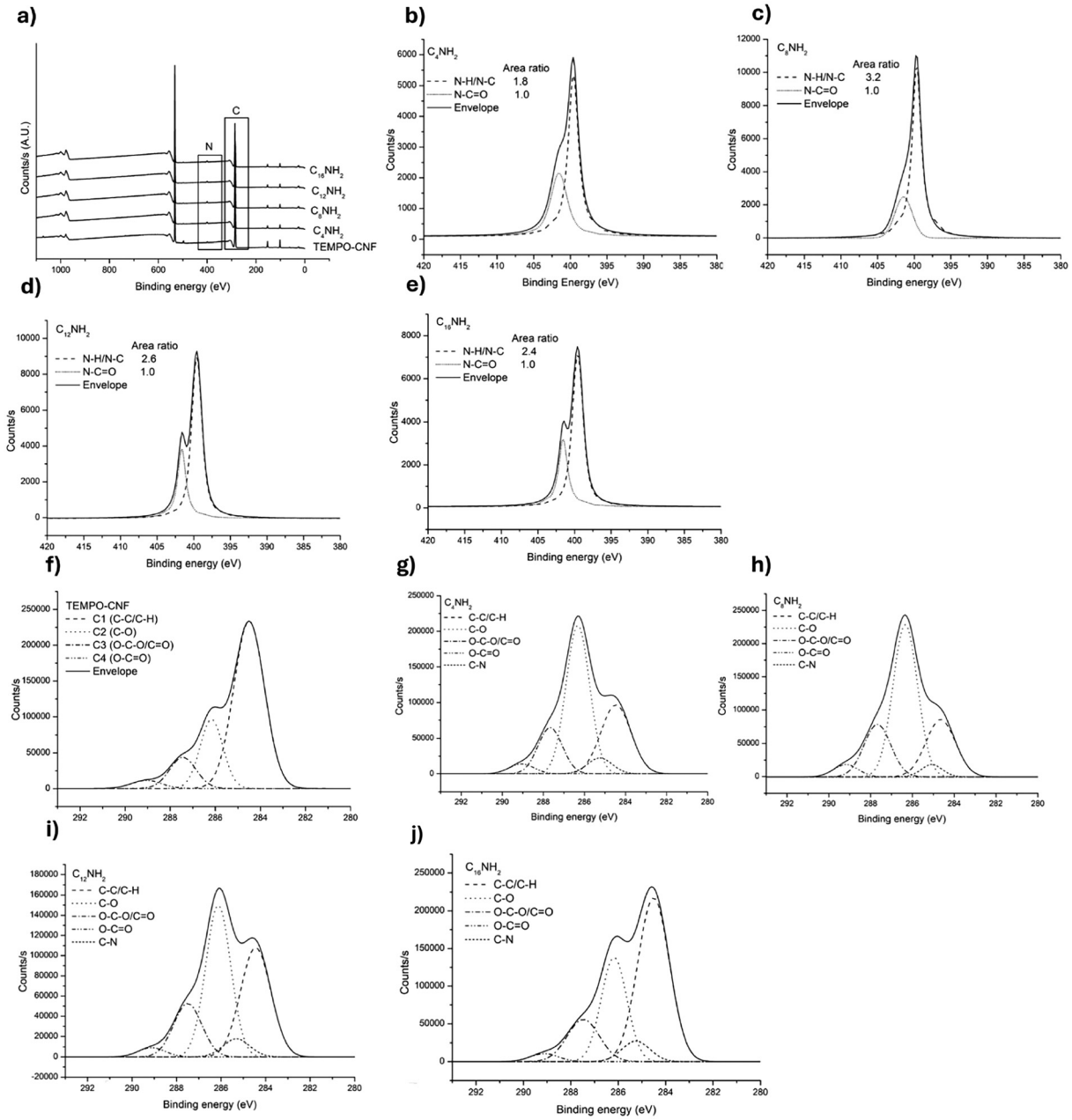

Fig. 2 (a) XPS spectra of the F0 and $C_{4-16}NH_2$ samples; (b–e) N 1s signal deconvolution of the $C_{4-16}NH_2$ samples; (f–j) C 1s signal deconvolution of the F0 and $C_{4-16}NH_2$ samples.

Table 3 XPS results

Film	O (%)	C (%)	N (%)	C–C/C–H (%)	C–N (%)	C–O (%)	O–C–O (%)	O–C═O (%)	O/C	N/O	DSS
F0	—	—	—	67 (25[a])	—	24	8	2	0.28	0.0266	—
C_4-NH_2	34.1	65.0	0.9	28.2	5.4	47.6	15.4	3.4	0.51	0.0274	0.11
C_8-NH_2	33.0	65.5	1.6	22.9	3.5	50.4	19.1	4.1	0.49	0.0458	0.21
C_{12}-NH_2	29.9	68.4	1.8	35.4	5.2	40.7	16.0	2.7	0.42	0.0584	0.26
C_{16}-NH_2	22.7	75.9	1.4	51.8	5.8	26.6	13.5	2.3	0.31	0.0683	0.21

[a] As reported by Chiulan *et al.*, 2021.[48]

Table 4 Correlation between the coefficient of diffusion of free amines and the DSS/DS ratio

Amine	D (10^{-6} cm^2 s^{-1})	DSS/DS
Butylamine	7.00	1.1
Octylamine	3.30	1.7
Dodecylamine	1.85	2.2
Hexadecylamine	0.99	1.9

and a roughness of TEMPO-CNF films, expressed as an arithmetic average (R_a), of 1.22 nm. A representative AFM picture of the C_{16}-NH_2 sample is shown in Fig. 3f.

Surface properties of amidated TEMPO-CNF films (water contact angle and surface energy)

Water contact angle (θ_w) measurements (Fig. 4a) confirmed the effectiveness of surface grafting, as all modified films showed reduced wettability compared to the control sample F0 (54.6° ± 6.3°). Among them, C_{16}-NH_2 exhibited the most pronounced effect, with a contact angle of 88.3° ± 0.6°, corresponding to an increase of 61% compared to F0. C_8-NH_2 (80.9° ± 0.3°) and C_{12}-NH_2 (82.2° ± 0.1°) also showed a notable increase, while C_4-NH_2 (60.0° ± 3.6°) did not differ significantly from the control ($p > 0.05$). The limited effect observed for C_4-NH_2 can likely be attributed to its short alkyl chain and to the more homogeneous functionalisation throughout the film, as suggested by elemental analysis and XPS, which indicate a DSS/DS ratio close to 1. In contrast, longer-chain amines (C_8–C_{16}) showed surface accumulation within the first ~10 nm of the film, leading to a higher surface concentration of hydrophobic alkyl groups and thus a more substantial reduction in wettability. To further characterize the surface properties, surface energy measurements were performed using the Owens–Wendt method and an apolar solvent (diiodomethane)[50] (see the SI), to quantitatively evaluate the nature of surface interactions on the films. These interactions may be polar, due to H-bond, dipole–dipole or ion–dipole, or dispersive, due to hydrophobic interactions. Data show that the polar component significantly decreased from 15.1 ± 0.3 mJ m^{-2} for F0 to 1.6 ± 0.6 mJ m^{-2} for C_{16}-NH_2 (see Fig. 4b), evidencing a progressive increase in hydrophobicity of the films, due to the presence of longer alkyl chains, generating van der Waals and/or London interactions. These findings demonstrate that grafting with amines having longer alkyl chains effectively reduces surface wettability (Fig. 4c) and polar surface energy of TEMPO-CNF films, thereby enhancing their hydrophobic character and potential performance in moisture-sensitive applications.

Gas barrier properties of amidated TEMPO-CNF films (MU%-WVP-OP)

Moisture uptake (MU%) was the first key parameter studied to evaluate the effect of TEMPO-CNF surface grafting on the film

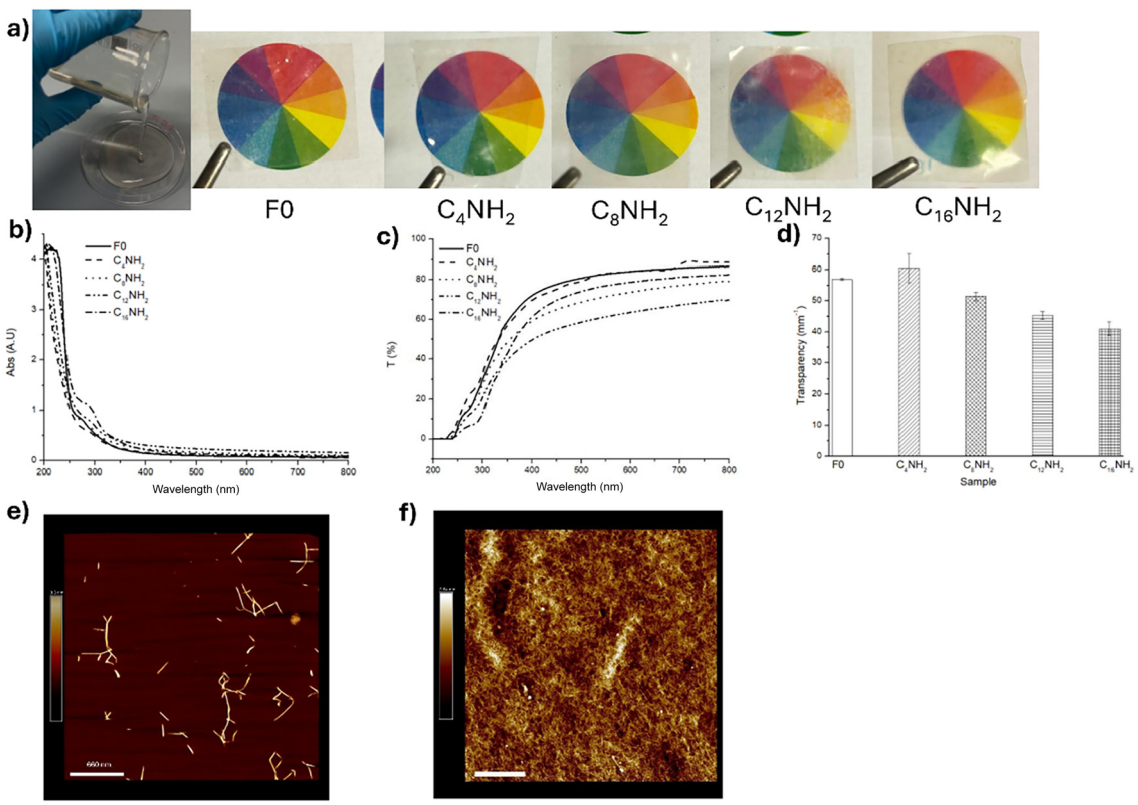

Fig. 3 (a) Film casting and graphical picture of the F0 and C_{4-16}-NH_2 grafted samples; UV-vis spectra of F0 and C_{4-16}-NH_2 in (b) absorbance and (c) transmittance; (d) transparency measurements; (e) AFM picture of TEMPO-CNF fibers; and (f) AFM picture of C_{16}-NH_2.

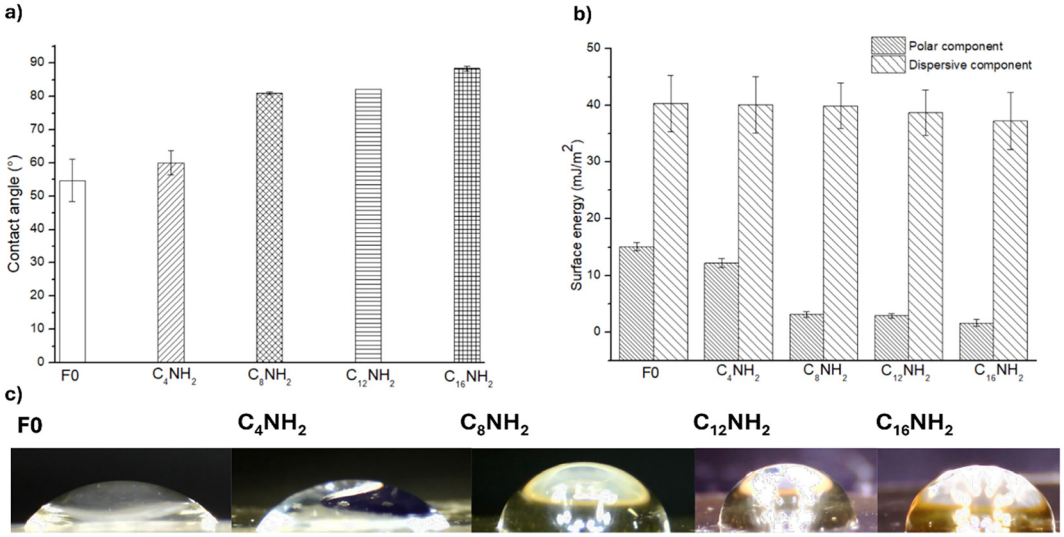

Fig. 4 (a) Water contact angle; (b) surface energy; (c) picture of the water contact angle of F0 and C_{4-16}-NH_2.

properties (Fig. 5a). The control sample F0 showed a MU% of 23.6 ± 0.3%, while the grafted films exhibited promising results with all amines used (C_4-NH_2: 12.7 ± 0.8%, C_8-NH_2: 11.9 ± 0.3%, C_{12}-NH_2: 10.4 ± 0.5%, C_{16}-NH_2: 8.5 ± 1.7%). As expected, the moisture uptake decreased as the alkyl chain length of the amine increased, from butylamine (C_4-NH_2) to hexadecylamine (C_{16}-NH_2). Interestingly, no reduction in MU% was observed for C_4-NH_2B (see the SI), providing further evidence that DMTMM is necessary for the formation of covalent bonds, which play a crucial role in enhancing the properties of the films. This confirms that surface grafting reduces the polarity of the surface by converting carboxylate groups into amidic groups bearing apolar alkyl chains.

Solala and coworkers[51] investigated the hydrophobic treatment of nano fibrillated cellulose (CNF) films *via* surface modification using C_{14}-alkylpolyethoxy-glycidylether, achieving approximately a 36% reduction in MU at 75% relative humidity (RH). Similarly, Sehaqui and coworkers[52] chemically grafted CNF with various anhydrides (acetic, butyric, hexanoic, and 2-dodecen-1-yl-succinic anhydride), followed by solvent

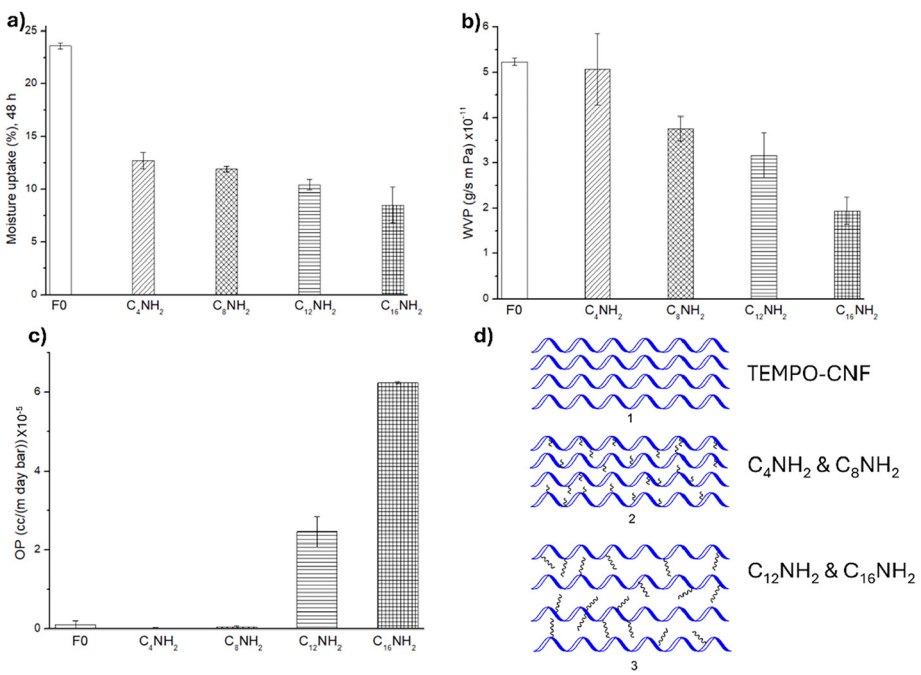

Fig. 5 (a) MU% at 98% RH and (b) WVP at 75% RH of F0 and C_4-NH_2–C_{16}-NH_2, (c) OP at 0% RH of F0 and C_4-NH_2, and (d) alkyl chain effect on OP.

exchange purification, reporting a moderate 30% improvement in MU at 85% RH compared to pristine CNF. In contrast, the TEMPO-CNF-*g*-amine films prepared in this study were obtained through a simpler protocol, yielding superior MU reductions, up to 50% for C_{16}-NH_2 at 97% RH. A comparison of the functional properties between the materials developed in this work and other hydrophobically modified nanocellulose-based materials is reported in Table 5.

To evaluate the barrier properties of functionalised films, water vapor permeability (WVP) measurements were performed. In agreement with contact angle measurements, the WVP of C_4-NH_2 ($5.07 \pm 0.79 \times 10^{-11}$ g s^{-1} m^{-1} Pa^{-1}) (Fig. 5b) showed no significant improvement compared to F0 ($5.23 \pm 0.08 \times 10^{-11}$ g s^{-1} m^{-1} Pa^{-1}) ($p > 0.05$). However, C_8-NH_2, C_{12}-NH_2, and C_{16}-NH_2 exhibited significant improvements, with WVP values of $3.76 \pm 0.27 \times 10^{-11}$ g s^{-1} m^{-1} Pa^{-1}, $3.17 \pm 0.50 \times 10^{-11}$ g s^{-1} m^{-1} Pa^{-1}, and $1.94 \pm 0.30 \times 10^{-11}$ g s^{-1} m^{-1} Pa^{-1}, respectively. Once again, C_{16}-NH_2 gave the best performances, with a 63% reduction in WVP compared to F0. Literature data often show counterintuitive trends with respect to grafting. For example, Solala and coworkers[51] observed no significant change in WVP after modifying CNFs with long alkyl-chain epoxides, despite increased hydrophobicity measured using the contact angle. Similarly, Shimizu and coworkers[53] reported a doubling of the contact angle (from 50° to 100°) for alkylammonium ionically surface-grafted TEMPO-CNF films, yet these showed decreased WVP performance relative to pristine TEMPO-CNF.

Oxygen permeability (OP) is another critical parameter for assessing the gas barrier performances of packaging materials. The non-functionalised TEMPO-CNF film (F0) exhibited a relatively low OP value of $(0.1 \pm 0.1) \times 10^{-5}$ cc m^{-1} bar^{-1} day^{-1}, reflecting the excellent intrinsic oxygen barrier properties of the nanocellulose network. This behaviour is primarily due to the highly ordered structure of the fibrils, reinforced by extensive hydrogen bonding, which effectively hinders gas diffusion through the material (Fig. 5d, entry 1). However, the inherent hydrophilicity of unmodified films substantially limits their applicability. To overcome this limitation, surface functionalisation was employed to enhance water resistance while preserving barrier performance. Interestingly, films grafted with butylamine (C_4NH_2) and octylamine (C_8-NH_2) showed statistically equivalent OP values ($p > 0.05$) ($(0.02 \pm 0.01) \times 10^{-5}$ cc m^{-1} bar^{-1} day^{-1} and $(0.04 \pm 0.03) \times 10^{-5}$ cc m^{-1} bar^{-1} day^{-1}, respectively), compared to F0.

These results suggest that alkyl chains of intermediate length do not compromise the oxygen barrier properties of TEMPO-CNF films (Fig. 5d, entry 2). This is probably due to the ability of these chains to occupy and fill nano- and micropores within the cellulose network, without disrupting the supramolecular order. Conversely, the statistically relevant, yet modest, increase in OP ($p < 0.05$) was observed for films modified with longer alkyl chains ($(2.46 \pm 0.38) \times 10^{-5}$ cc m^{-1} bar^{-1} day^{-1} and $(6.24 \pm 0.03) \times 10^{-5}$ cc m^{-1} bar^{-1} day^{-1} for C_{12}-NH_2 and C_{16}-NH_2, respectively), indicating a slight loss in barrier efficiency. This behaviour may be attributed to several structural effects introduced by longer, more flexible alkyl chains. First, their bulkiness may generate additional free volume and reduce the overall packing density of the fibril network, thereby facilitating oxygen diffusion (Fig. 5d). Second, the protonated amine groups of the grafted moieties may act as surfactant-like agents, promoting partial diffusion of the hydrophobic chains into the film bulk. This could locally disturb the molecular order of the fibrils and disrupt the tight, layered structure that contributes to low permeability. Additionally, the presence of excess hydrophobic groups may weaken the hydrogen bonding interactions critical to maintaining the dense fibrillar architecture. Taken together, these findings highlight the dual role of the grafted alkyl chains: while their hydrophobic nature enhances water resistance and contributes to filling surface voids, their size must be carefully balanced to avoid compromising the oxygen barrier function.

Finally, it is worth noting that WVP and OP respond differently to chemical modifications. The WVP appears to be primarily governed by the hydrophobic/apolar character of the surface, whereas the OP is more sensitive to the steric effects

Table 5 Literature comparison between the starting material and the best-performing grafted material

	MU%			WU%			θ_w (°)			WVP		
Sample	M0[a]	MF[b]	Δ[c]	M0[a]	MF[b]	Δ[c]	M0[a]	MF[b]	Δ[c]	M0[a]	MF[b]	Δ[c]
This work	26.3 ± 0.3	8.5 ± 1.7	−50%	1670 ± 47	26.2 ± 3.0	−98%	54.6 ± 6.3	88.3 ± 0.6	+61%	5.23 ± 0.08[d]	1.94 ± 0.30[d]	−63%
51[j]	14[e]	9[e]	−36%	—	—	—	25	55	+120%	910[f]	820[f]	−0%
52[k]	~17.5[g]	~12.0[g]	−30%[b]	—	—	—	23.9	118.5	+395%	—	—	—
53[l]	—	—	—	—	—	—	50	100	+100%	22[h]	30[h]	+26%
54[m]	—	—	—	~90	~6	−93%	54 ± 2	101 ± 2	+87%	9.02 ± 0.18[i]	3.40 ± 0.09[i]	−62%
55[n]	—	—	—	900	80	−91%	—	—	—	—	—	—

All values refer to relative differences between the chemically functionalised sample compared to the starting material. [a] M0: starting material. [b] MF: best-performing functionalised material. [c] Δ: relative variation. [d] 10^{-11} g s^{-1} m^{-1} Pa^{-1}. [e] 80% RH. [f] WVTR values (g m^{-2} day^{-1}). [g] 85% RH. [h] 10^3 ml μm m^{-2} day^{-1}. [i] RH 100%; 10^{-9} g m^{-1} s^{-1} Pa^{-1}. [j] M0: CNF, MF: CNF functionalised with C14-alkylpolyethoxy-glycidylether. [k] M0: CNF, MF: CNF functionalised with 2 dodecen-1-yl-succinnic anhydride. [l] M0: TEMPO-CNF, MF: TEMPO CNF functionalised with quaternary ammonium salt. [m] M0: CNF, MF: CNF functionalized with10-undecylenoyl chloride. [n] M0: TEMPO-CNF, MF: TEMPO CNF crosslinked with epichlorohydrin and $CaCl_2$.

and packing disruption caused by the alkyl chain length. These findings align with previous work by Bras and co-workers,[56] who observed similar trends in fully substituted cellulose ester films containing long alkyl chains. Nevertheless, the OP value of C_{16}-NH_2 and C_{12}-NH_2 films still reflects adequate barrier performances for potential packaging applications,[57] especially considering the bio-based nature of the material and the significant improvement in water-resistance properties achieved. It is important to note that all OP measurements were performed at 0% relative humidity. TEMPO-CNF films are well known to suffer from a significant loss in barrier properties at high humidity levels due to water vapor sorption,[25] which induces fiber swelling, disrupts the tight hydrogen-bonding network, and increases the free volume for gas transport. However, the covalent functionalisation with aliphatic amines presented here is expected to actively mitigate this performance drop through two main mechanisms. First, the conversion of hydrophilic carboxylate groups into hydrophobic amide groups reduces the overall number of primary water-binding sites. Second, the alkyl chains (especially for longer chains like C_8–C_{12}) form a hydrophobic surface layer (as evidenced by the sharp increase in water contact angle) that acts as a physical shield, slowing down the diffusion of water molecules into the bulk network. While a comprehensive investigation of the OP at variable RH% (*e.g.*, 50% and 85% RH) is essential to fully quantify the performance in real-life packaging environments, the chemical and structural changes observed in this study strongly evidence an enhanced moisture-resistance barrier.

Film–water interaction of amidated TEMPO-CNF films (WS%, WU% and WP)

One of the main limitations of TEMPO-CNF films is their poor water stability, due to their highly hydrophilic nature which leads to fiber redispersion upon water exposure. To evaluate the impact of surface grafting on this behaviour, water stability (WS%) tests were conducted. The results were highly promising: F0 exhibited a mass loss of 26.9 ± 4.3% after 24 hours of static water immersion, whereas the grafted films showed significantly lower mass losses: 8.9 ± 0.4% for C_4-NH_2, 3.2 ± 0.6% for C_8-NH_2, 5.0 ± 0.8% for C_{12}-NH_2, and 5.3 ± 1.9% for C_{16}-NH_2. A marked reduction in WS% was observed between F0 and C_4-NH_2 (66% decrease, $p < 0.05$), while the WS% values reached a plateau between 3.2% and 5.3% with longer alkyl chains ($p > 0.05$; Fig. 6a).

Water uptake (WU%, Fig. 6b) experiments confirmed the beneficial effect of surface grafting. All grafted films (C_4-NH_2, C_8-NH_2, C_{12}-NH_2, and C_{16}-NH_2) showed a significant reduction in WU% compared to the control F0. After 120 minutes of immersion, F0 exhibited a WU% value of (1670 ± 47)%, whereas the grafted samples had much lower values: 236.7 ± 5.0% (C_4-NH_2), 91.8 ± 2.2% (C_8-NH_2), 38.9 ± 3.5% (C_{12}-NH_2), and 26.2 ± 3.0% (C_{16}-NH_2). Notably, the non-covalently bonded sample C_4-NH_2B performed significantly worse than

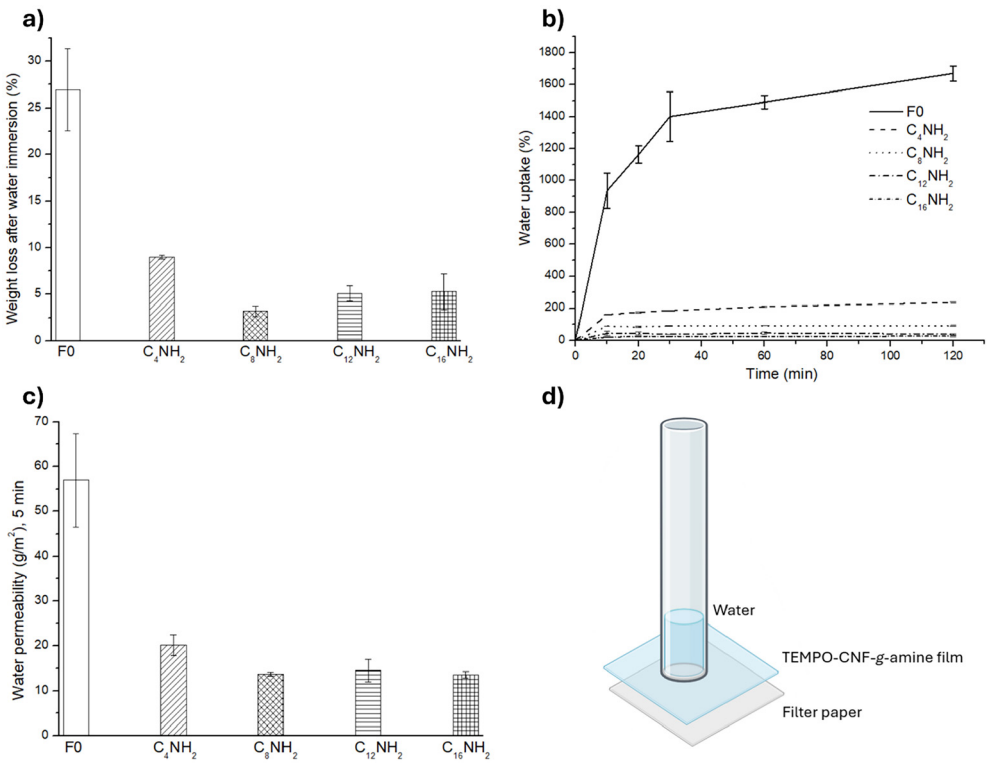

Fig. 6 (a) Water stability; (b) water uptake; (c) water permeability; and (d) schematic experimental setup for WP measurements.

C_4-NH_2, highlighting once more the crucial role of covalent bonding (see the SI). Therefore, no further investigations were carried out on C_4-NH_2B. This further supports the importance of the covalent bonds formed through the DMTMM-mediated reaction in enhancing the surface properties of the films. The best performances were observed for the C_{16}-NH_2 grafted films, which achieved a reduction in WU of 98% compared to F0. Lee and coworkers[55] reported a double crosslinking strategy of TEMPO-CNF using epichlorohydrin and calcium chloride, achieving a 91% reduction in WU compared to pristine TEMPO-CNF. This is comparable to the WU reduction reported in this work with C_{16}-NH_2 films, yet, notably without the use of epichlorohydrin. Li and coworkers[54] described grafting of CNF with 10-undecylenoyl chloride in the presence of pyridine as the catalyst, at 80 °C for 1 h in dimethylacetamide as the solvent, followed by vacuum filtration. These modified CNF films exhibited a 93% decrease in WU, an increase in contact angle from 54° to 101°, and a 62% reduction in WVP, which are consistent with the results reported here.

Additionally, water permeability (WP, Fig. 6c) tests were performed using a self-built setup (Fig. 6d) to assess the barrier performance of the films in direct contact with water. Despite the severe test conditions, the grafted films showed substantial improvements in WP compared to F0 (57 ± 10 g m^{-2}) regardless of the alkyl chain length. C_4-NH_2 displayed a WP of 20 ± 2 g m^{-2}, while C_8-NH_2, C_{12}-NH_2, and C_{16}-NH_2 exhibited similar or even lower values. Overall, functionalised films achieved a WP reduction of approximately 77%, with the lowest value for C_{16}-NH_2 (13.5 ± 0.7 g m^{-2}). These results clearly demonstrate that covalent grafting of hydrophobic amines significantly enhances the water resistance and barrier properties of TEMPO-CNF films, making them viable candidates for applications in humid or aqueous environments.

Influence of fiber functionalisation on biofragmentation

Biofragmentation of the films was evaluated through soil burial tests carried out on both F0 and all TEMPO-CNF-*g*-amine films prepared. Samples were periodically recovered from the soil, gently rinsed to remove residual particles, dried, and weighed at scheduled time points. The test was carried out over a total period of 24 weeks (6 months). For this type of analysis, it should be noted that the biofragmentation observed in soil burial tests represents only the initial stage of a complete biodegradation process. During this phase, physical and biological agents promote polymer chain scission, breaking the material down into smaller chemical species. Rigorously speaking, true biodegradation can only be confirmed by quantifying the carbon dioxide evolved during the process.[58]

Therefore, while these soil burial experiments, based on visual inspection and weight loss analysis, provide useful indicative information regarding the environmental fate of the material, they specifically demonstrate its biofragmentation rather than standard biodegradation. Representative images of film appearance during degradation are shown in Fig. 7a, and the corresponding weight loss over time is reported in Fig. 7b. F0 displayed rapid and complete biofragmentation within just two weeks. This fast degradation is a consequence of the high hydrophilicity of the material, which facilitates the diffusion of water and enzymatic activity within the film matrix. In particular, the presence of a high concentration of hydroxyl and carboxylate groups in cellulose quickly enables microbial hydrolysis of the glycosidic bonds, leading to rapid disintegration. The grafting of hydrophobic alkyl chains through amide surface functionalisation significantly affects the degradation kinetics. In fact, the biofragmentation process slows down as the alkyl chain length increases. Films modified with butylamine (C_4-NH_2) degraded completely within 8 weeks, while substantial disintegration of those modified with octylamine (C_8-NH_2) occurred within 24 weeks. In contrast, films grafted with dodecylamine (C_{12}-NH_2) and hexadecylamine (C_{16}-NH_2) showed incomplete degradation even after 24 weeks with this method.

In addition to the slower weight loss, these long-chain modified films also exhibited a progressive yellowing during soil burial, indicating possible oxidative processes or accumulation of degraded by-products on the film surface. This trend confirms that hydrophobic functionalisation limits water and enzyme penetration, with longer alkyl chains providing stron-

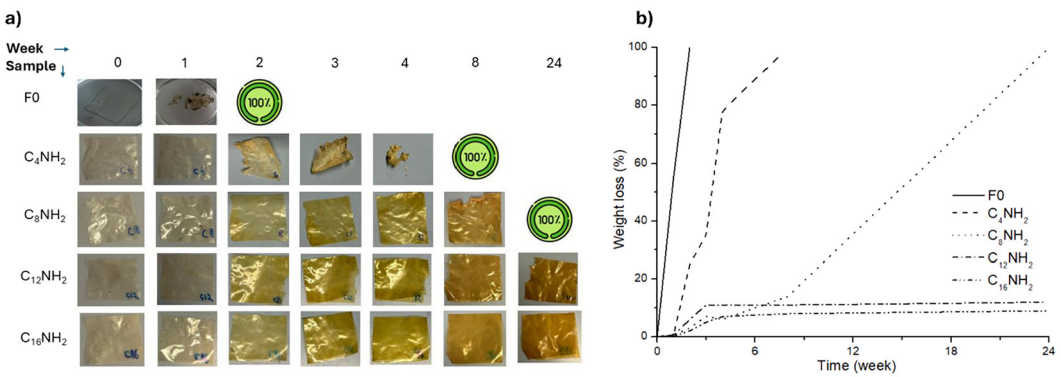

Fig. 7 (a) Graphical visualization of the biofragmentation process and (b) weight loss due to biofragmentation as a function of time.

ger shielding and thereby reducing enzymatic degradation. Some methodological limitations may have influenced the results. Specifically, periodic removal, washing, and drying of the samples for weight measurements could have interfered with the natural degradation process by temporarily interrupting microbial activity or altering the film surface. Moreover, the test conditions applied in this work (25 °C, aerobic exposure, 50% relative humidity) do not correspond to standardized protocols for assessing biodegradability or composability. According to EN ISO 17556:2019, a maximum test duration of 6 months under defined soil conditions is required for materials to be classified as biodegradable in soil, while other standards such as EN 13432:2002 (industrial composting, 58 °C, high humidity, forced aeration) and EN 13432:2022 (home composting) define different requirements. Therefore, the results presented here should be regarded only as a preliminary and approximate indication of the films' degradation behaviour. They nevertheless suggest that samples with longer alkyl chains exhibit higher resistance, which is advantageous for certain applications, but does not exclude the possibility that these materials could still be compostable under industrial conditions and will be the object of future studies.

Conclusion

In this study, a novel and sustainable strategy for the amidation of TEMPO-CNF films *via* soaking in the presence of DMTMM as a coupling agent has been successfully developed. The reactions were carried out under mild conditions in a sustainable water–ethanol solvent system, confirming the feasibility of this approach for eco-friendly surface functionalisation. A series of alkylamines with increasing alkyl chain lengths (C_4, C_8, C_{12}, and C_{16}) were employed to evaluate the influence of hydrophobic moieties on the material properties. Chemical grafting was confirmed through ATR FT-IR and XPS analyses, demonstrating successful covalent functionalisation of the TEMPO-CNF surface. The correlation found between the amine diffusion coefficients and both DSS and DS elucidates the interfacial confinement of long-chain amines, turning a simple hydrophobization process into a predictable, highly efficient surface-engineering strategy.

Importantly, the functionalised films largely retained the good optical properties of TEMPO-CNF, with only a moderate reduction in transparency. Notably, chemical modification led to an overall enhancement of the water resistance and water barrier properties when amines with longer alkyl chains (C_{12}, C_{16}) were grafted. Furthermore, the excellent oxygen barrier properties of TEMPO-CNF were largely preserved after grafting and only a moderate increase in OP was observed for the longer alkyl chains.

However, some critical issues emerged that deserve further investigation. Retention of non-covalently adsorbed long-alkyl chain amines on the film surface after grafting remains a potential concern for packaging applications. Dedicated release tests should be performed to assess the stability of the functionalization and the risk of amine leaching during use. Furthermore, while C_4-NH_2 and C_8-NH_2 samples showed relatively fast biofragmentation, the process was incomplete after 24 weeks for C_{12}-NH_2 and C_{16}-NH_2 films under soil conditions (25 °C, 50% RH). More comprehensive biodegradation tests under composting conditions are needed to fully understand the environmental fate of these materials.

In conclusion, this work provides a solid proof of concept for a simple, green, and effective strategy to tailor the surface properties of TEMPO-CNF films. At the same time, it highlights the importance of further studies to address long-term stability and biodegradability, which are essential for real-world applications and sustainable packaging development.

Author contributions

D. S. contributed to conceptualization, formal analysis, data curation, experimental investigation, methodology, validation, visualization, funding acquisition, writing – original draft, and writing – review and editing; C. S. contributed to formal analysis, validation, and writing – review and editing; C. R. contributed to formal analysis, validation, experimental investigation, and methodology; V. B. contributed to funding acquisition, validation, and writing – review and editing; J. B. contributed to conceptualization, formal analysis, funding acquisition, methodology, validation, and writing – review and editing.

Conflicts of interest

The authors declare no competing financial interests.

Data availability

All data supporting the findings of this study are available within the article and its supplementary information (SI). The Supporting Information contains the moisture uptake and water uptake comparison between F0, C_4NH_2, and C_4NH_2B, the contact angle values for surface energy calculation, and the experimental XPS data of F0 and C_4-$C_{16}NH_2$ samples. Additionally, the XPS data fitting and the OTR raw data are provided. Supplementary information is available. See DOI: https://doi.org/10.1039/d6py00462h.

Acknowledgements

This work was supported by PNRR funding for the 38th PhD cycle "Dottorato di Interesse Nazionale in Desing per il Made in Italy: Identità, Innovazione e Sostenibilità", administrative headquarter University of Campania "Luigi Vanvitelli", Caserta (Italy).

Part of the work was carried out in the LGP2 (France) thanks to the Erasmus + Traineeship Program. The LGP2 is part of the

LabEx Tec 21 (grant agreement no. ANR-11-LABX-0030), the Institut Carnot Polynat (grant agreement no. ANR-16-CARN-002501) and the Cross disciplinary program Glyco@Alps (Investissements d'avenir – grant agreement ANR-15-IDEX-02). This work was supported by the French Government through the Laboratoire d'Excellence CEMAM (no. ANR-10-LABX-44-01) within the program Investissements d'Avenir.

References

1 R. C. Thompson, W. Courtene-Jones, J. Boucher, S. Pahl, K. Raubenheimer and A. A. Koelmans, Twenty Years of Microplastic Pollution Research—What Have We Learned?, *Science*, 2024, **386**(6720), eadl2746, DOI: 10.1126/science.adl2746.

2 J. R. Jambeck, R. Geyer, C. Wilcox, T. R. Siegler, M. Perryman, A. Andrady, R. Narayan and K. L. Law, Plastic Waste Inputs from Land into the Ocean, *Science*, 2015, **347**(6223), 768–771, DOI: 10.1126/science.1260352.

3 V. Beghetto, V. Gatto, R. Samiolo, C. Scolaro, S. Brahimi, M. Facchin and A. Visco, Plastics Today: Key Challenges and EU Strategies towards Carbon Neutrality: A Review, *Environ. Pollut.*, 2023, **334**, 122102, DOI: 10.1016/j.envpol.2023.122102.

4 R. Marfella, F. Prattichizzo, C. Sardu, G. Fulgenzi, L. Graciotti, T. Spadoni, N. D'Onofrio, L. Scisciola, R. La Grotta, C. Frigé, V. Pellegrini, M. Municinò, M. Siniscalchi, F. Spinetti, G. Vigliotti, C. Vecchione, A. Carrizzo, G. Accarino, A. Squillante, G. Spaziano, D. Mirra, R. Esposito, S. Altieri, G. Falco, A. Fenti, S. Galoppo, S. Canzano, F. C. Sasso, G. Matacchione, F. Olivieri, F. Ferraraccio, I. Panarese, P. Paolisso, E. Barbato, C. Lubritto, M. L. Balestrieri, C. Mauro, A. E. Caballero, S. Rajagopalan, A. Ceriello, B. D'Agostino, P. Iovino and G. Paolisso, Microplastics and Nanoplastics in Atheromas and Cardiovascular Events, *N. Engl. J. Med.*, 2024, **390**(10), 900–910, DOI: 10.1056/nejmoa2309822.

5 S. Liu, Z. Low, Z. Xie and H. Wang, TEMPO-Oxidized Cellulose Nanofibers: A Renewable Nanomaterial for Environmental and Energy Applications, *Adv. Mater. Technol.*, 2021, **6**(7), 2001180, DOI: 10.1002/admt.202001180.

6 C. Johansson, J. Bras, I. Mondragon, P. Nechita, D. Plackett, P. Šimon, D. Gregor Svetec, S. Virtanen, M. Giacinti Baschetti, C. Breen and S. Aucejo, RENEWABLE FIBERS AND BIO-BASED MATERIALS FOR PACKAGING APPLICATIONS – A REVIEW OF RECENT DEVELOPMENTS, *BioRes*, 2012, **7**(2), 2506–2552, DOI: 10.15376/biores.7.2.2506-2552.

7 A. Visco, C. Scolaro, M. Facchin, S. Brahimi, H. Belhamdi, V. Gatto and V. Beghetto, Agri-Food Wastes for Bioplastics: European Prospective on Possible Applications in Their Second Life for a Circular Economy, *Polymers*, 2022, **14**(13), 2752, DOI: 10.3390/polym14132752.

8 V. Beghetto, S. Conca and D. Santandrea, Carboxymethyl Cellulose-Based Films for Sustainable Food Packaging: Modification Strategies and Structure–Property Relationships, *Polymers*, 2026, **18**(5), 552, DOI: 10.3390/polym18050552.

9 A. Visco, C. Scolaro, S. Brahimi, S. Conca and V. Beghetto, Effect of α-Tocopherol on the Processability, Tensile Properties, and Structure of Fully Bio-Based Poly (Butylene Succinate)/Brewer's Spent Grain Composites, *Mater. Today Commun.*, 2026, **53**, 115413, DOI: 10.1016/j.mtcomm.2026.115413.

10 D. Santandrea, J. Caldato and V. Beghetto, Amidated Carboxymethylcellulose: Synthesis, Characterization and Evaluation of Their Performance in Paper Coating Application, *Cellulose*, 2026, **33**(1), 481–503, DOI: 10.1007/s10570-025-06769-4.

11 N. Canzian, G. Foltran and V. Beghetto, Turning Unsorted Stranded Seaweeds into Biocomposites, *Mater. Today Commun.*, 2026, **52**, 115228, DOI: 10.1016/j.mtcomm.2026.115228.

12 P. Cazón, G. Velazquez, J. A. Ramírez and M. Vázquez, Polysaccharide-Based Films and Coatings for Food Packaging: A Review, *Food Hydrocolloids*, 2017, **68**, 136–148, DOI: 10.1016/j.foodhyd.2016.09.009.

13 J. Vartiainen, M. Vähä-Nissi and A. Harlin, Biopolymer Films and Coatings in Packaging Applications—A Review of Recent Developments, *Mater. Sci. Appl.*, 2014, **05**(10), 708–718, DOI: 10.4236/msa.2014.510072.

14 Y. A. Shah, S. Bhatia, A. Al-Harrasi and T. S. Khan, Advancements in the Biopolymer Films for Food Packaging Applications: A Short Review, *Biotechnol. Sustainable Mater.*, 2024, **1**(1), 2, DOI: 10.1186/s44316-024-00002-1.

15 H. N. Abdelhamid and A. P. Mathew, Cellulose-Based Materials for Water Remediation: Adsorption, Catalysis, and Antifouling, *Front. Chem. Eng.*, 2021, **3**, 790314, DOI: 10.3389/fceng.2021.790314.

16 A. Visco, N. Bardella, C. Scolaro, H. Belhamdi, S. Brahimi, V. Gatto, R. Samiolo and V. Beghetto, Reuse of Beer Spent Grain for the Industrial Production of Biodegradable Bio-Composites, *Ind. Crops Prod.*, 2025, **235**, 121684, DOI: 10.1016/j.indcrop.2025.121684.

17 D. Roy, M. Semsarilar, J. T. Guthrie and S. Perrier, Cellulose Modification by Polymer Grafting: A Review, *Chem. Soc. Rev.*, 2009, **38**(7), 2046, DOI: 10.1039/b808639g.

18 S. Acharya, S. Liyanage, P. Parajuli, S. S. Rumi, J. L. Shamshina and N. Abidi, Utilization of Cellulose to Its Full Potential, A Review on Cellulose Dissolution, Regeneration, and Applications, *Polymers*, 2021, **13**(24), 4344, DOI: 10.3390/polym13244344.

19 E. Freville, J. Pescheux-Sergienko, R. Mujica, C. Rey and J. Bras, Novel Technologies for Producing Tridimensional Cellulosic Materials for Packaging: A Review, *Carbohydr. Polym.*, 2024, **342**, 122413, DOI: 10.1016/j.carbpol.2024.122413.

20 R. Ramakrishnan, J. T. Kim, S. Roy and A. Jayakumar, Recent Advances in Carboxymethyl Cellulose-Based Active and Intelligent Packaging Materials: A Comprehensive

Review, *Int. J. Biol. Macromol.*, 2024, **259**, 129194, DOI: 10.1016/j.ijbiomac.2023.129194.

21 L. S. F. Leite, M. Le Gars, H. M. C. Azeredo, F. K. V. Moreira, L. H. C. Mattoso and J. Bras, Insights into the Effect of Carboxylated Cellulose Nanocrystals on Mechanical and Barrier Properties of Gelatin Films for Flexible Packaging Applications, *Int. J. Biol. Macromol.*, 2024, **280**, 135726, DOI: 10.1016/j.ijbiomac.2024.135726.

22 N. Lavoine, I. Desloges, A. Dufresne and J. Bras, Microfibrillated Cellulose – Its Barrier Properties and Applications in Cellulosic Materials: A Review, *Carbohydr. Polym.*, 2012, **90**(2), 735–764, DOI: 10.1016/j.carbpol.2012.05.026.

23 S. Paganelli, N. Massimi, A. Di Michele, O. Piccolo, R. Rampazzo, M. Facchin and V. Beghetto, Use of Carboxymethyl Cellulose as Binder for the Production of Water-Soluble Catalysts, *Int. J. Biol. Macromol.*, 2024, **270**, 132541, DOI: 10.1016/j.ijbiomac.2024.132541.

24 H. P. S. Abdul Khalil, Y. Davoudpour, M. N. Islam, A. Mustapha, K. Sudesh, R. Dungani and M. Jawaid, Production and Modification of Nanofibrillated Cellulose Using Various Mechanical Processes: A Review, *Carbohydr. Polym.*, 2014, **99**, 649–665, DOI: 10.1016/j.carbpol.2013.08.069.

25 C. Aulin, M. Gällstedt and T. Lindström, Oxygen and Oil Barrier Properties of Microfibrillated Cellulose Films and Coatings, *Cellulose*, 2010, **17**(3), 559–574, DOI: 10.1007/s10570-009-9393-y.

26 A. Isogai, T. Saito and H. Fukuzumi, TEMPO-Oxidized Cellulose Nanofibers, *Nanoscale*, 2011, **3**(1), 71–85, DOI: 10.1039/C0NR00583E.

27 K. Missoum, M. Belgacem and J. Bras, Nanofibrillated Cellulose Surface Modification: A Review, *Materials*, 2013, **6**(5), 1745–1766, DOI: 10.3390/ma6051745.

28 R. K. Johnson, A. Zink-Sharp and W. G. Glasser, Preparation and Characterization of Hydrophobic Derivatives of TEMPO-Oxidized Nanocelluloses, *Cellulose*, 2011, **18**(6), 1599–1609, DOI: 10.1007/s10570-011-9579-y.

29 A. Kumar, B. Watbled, I. Baussanne, S. Hediger, M. Demeunynck and G. De Paëpe, Optimizing Chemistry at the Surface of Prodrug-Loaded Cellulose Nanofibrils with MAS-DNP, *Commun. Chem.*, 2023, **6**(1), 58, DOI: 10.1038/s42004-023-00852-2.

30 M. D'Este, D. Eglin and M. Alini, A Systematic Analysis of DMTMM vs EDC/NHS for Ligation of Amines to Hyaluronan in Water, *Carbohydr. Polym.*, 2014, **108**, 239–246, DOI: 10.1016/j.carbpol.2014.02.070.

31 R. Sole, C. Buranello, A. Di Michele and V. Beghetto, Boosting Physical-Mechanical Properties of Adipic Acid/Chitosan Films by DMTMM Cross-Linking, *Int. J. Biol. Macromol.*, 2022, **209**, 2009–2019, DOI: 10.1016/j.ijbiomac.2022.04.181.

32 V. Beghetto, V. Gatto, S. Conca, N. Bardella, C. Buranello, G. Gasparetto and R. Sole, Development of 4-(4,6-Dimethoxy-1,3,5-Triazin-2-Yl)-4-Methyl-Morpholinium Chloride Cross-Linked Carboxymethyl Cellulose Films, *Carbohydr. Polym.*, 2020, **249**, 116810, DOI: 10.1016/j.carbpol.2020.116810.

33 Y. Yoshikawa, K. Yamato, A. Ishida, Y. Yoshida, Y. Kumamoto and A. Isogai, Amidation of Carboxy Groups in TEMPO-Oxidized Cellulose for Improving Surface Hydrophobization and Thermal Stability of TEMPO-CNCs, *Carbohydr. Polym.*, 2025, **347**, 122654, DOI: 10.1016/j.carbpol.2024.122654.

34 V. Beghetto, L. Agostinis, V. Gatto, R. Samiolo and A. Scrivanti, Sustainable Use of 4-(4,6-Dimethoxy-1,3,5-Triazin-2-Yl)-4-Methylmorpholinium Chloride as Metal Free Tanning Agent, *J. Cleaner Prod.*, 2019, **220**, 864–872, DOI: 10.1016/j.jclepro.2019.02.034.

35 V. Gatto, S. Conca, N. Bardella and V. Beghetto, Efficient Triazine Derivatives for Collagenous Materials Stabilization, *Materials*, 2021, **14**(11), 3069, DOI: 10.3390/ma14113069.

36 D. Santandrea, C. Sillard, V. Beghetto and J. Bras, Aqueous-Phase Surface Amidation of TEMPO-CNF Films for Improved Adsorption of Organic Pollutants in Water, *ChemPlusChem*, 2025, 202500398, DOI: 10.1002/cplu.202500398.

37 D. Santandrea and V. Beghetto, 4-(4,6-Dimethoxy-1,3,5-Triazin-2-Yl)-4-Methyl-Morpholinium Chloride-Assisted Amide Crosslinking of Carboxymethyl Cellulose for High-Performing Films, *RSC Adv.*, 2025, **15**(42), 34846–34860, DOI: 10.1039/D5RA05273D.

38 M. Le Gars, A. Delvart, P. Roger, M. N. Belgacem and J. Bras, Amidation of TEMPO-Oxidized Cellulose Nanocrystals Using Aromatic Aminated Molecules, *Colloid Polym. Sci.*, 2020, **298**(6), 603–617, DOI: 10.1007/s00396-020-04640-5.

39 J. Pescheux-Sergienko, C. Sillard, M. N. Belgacem and J. Bras, Simultaneous Comminution and Hydrophobization of Cellulose Fibers by Mechanochemistry, *ACS Sustainable Chem. Eng.*, 2024, **12**(45), 16540–16552, DOI: 10.1021/acssuschemeng.4c04209.

40 C. Goussé, H. Chanzy, G. Excoffier, L. Soubeyrand and E. Fleury, Stable Suspensions of Partially Silylated Cellulose Whiskers Dispersed in Organic Solvents, *Polymer*, 2002, **43**(9), 2645–2651, DOI: 10.1016/S0032-3861(02)00051-4.

41 J. H. Han and J. D. Floros, Casting Antimicrobial Packaging Films and Measuring Their Physical Properties and Antimicrobial Activity, *J. Plast. Film Sheeting*, 1997, **13**(4), 287–298, DOI: 10.1177/875608799701300405.

42 R. J. C. Brown, The Use and Abuse of Limits of Detection in Environmental Analytical Chemistry, *Sci. World J.*, 2008, **8**, 796–801, DOI: 10.1100/tsw.2008.107.

43 S. Saini, C. Sillard, M. Naceur Belgacem and J. Bras, Nisin Anchored Cellulose Nanofibers for Long Term Antimicrobial Active Food Packaging, *RSC Adv.*, 2016, **6**(15), 12422–12430, DOI: 10.1039/C5RA22748H.

44 T. Borke, F. M. Winnik, H. Tenhu and S. Hietala, Optimized Triazine-Mediated Amidation for Efficient and Controlled Functionalization of Hyaluronic Acid,

Carbohydr. Polym., 2015, **116**, 42–50, DOI: 10.1016/j.carbpol.2014.04.012.

45 A. Heydari, N. Borazjani, F. Kazemi-Aghdam, J. Filo and I. Lacík, DMTMM-Mediated Amidation of Sodium Alginate in Aqueous Solutions: pH-Dependent Efficiency of Conjugation, *Carbohydr. Polym.*, 2025, **348**, 122893, DOI: 10.1016/j.carbpol.2024.122893.

46 M. Andresen, L.-S. Johansson, B. S. Tanem and P. Stenius, Properties and Characterization of Hydrophobized Microfibrillated Cellulose, *Cellulose*, 2006, **13**(6), 665–677, DOI: 10.1007/s10570-006-9072-1.

47 Z. Hu, R. M. Berry, R. Pelton and E. D. Cranston, One-Pot Water-Based Hydrophobic Surface Modification of Cellulose Nanocrystals Using Plant Polyphenols, *ACS Sustainable Chem. Eng.*, 2017, **5**(6), 5018–5026, DOI: 10.1021/acssuschemeng.7b00415.

48 I. Chiulan, D. M. Panaitescu, E.-R. Radu, S. Vizireanu, V. Sătulu, B. Biță, R. A. Gabor, C. A. Nicolae, M. Raduly and V. Rădițoiu, Influence of TEMPO Oxidation on the Properties of Ethylene Glycol Methyl Ether Acrylate Grafted Cellulose Sponges, *Carbohydr. Polym.*, 2021, **272**, 118458, DOI: 10.1016/j.carbpol.2021.118458.

49 N. Lavoine, J. Bras, T. Saito and A. Isogai, Improvement of the Thermal Stability of TEMPO-Oxidized Cellulose Nanofibrils by Heat-Induced Conversion of Ionic Bonds to Amide Bonds, *Macromol. Rapid Commun.*, 2016, **37**(13), 1033–1039, DOI: 10.1002/marc.201600186.

50 S. Rbihi, A. Aboulouard, L. Laallam and A. Jouaiti, Contact Angle Measurements of Cellulose Based Thin Film Composites: Wettability, Surface Free Energy and Surface Hardness, *Surf. Interfaces*, 2020, **21**, 100708, DOI: 10.1016/j.surfin.2020.100708.

51 I. Solala, R. Bordes and A. Larsson, Water Vapor Mass Transport across Nanofibrillated Cellulose Films: Effect of Surface Hydrophobization, *Cellulose*, 2018, **25**(1), 347–356, DOI: 10.1007/s10570-017-1608-z.

52 H. Sehaqui, T. Zimmermann and P. Tingaut, Hydrophobic Cellulose Nanopaper through a Mild Esterification Procedure, *Cellulose*, 2014, **21**(1), 367–382, DOI: 10.1007/s10570-013-0110-5.

53 M. Shimizu, T. Saito, H. Fukuzumi and A. Isogai, Hydrophobic, Ductile, and Transparent Nanocellulose Films with Quaternary Alkylammonium Carboxylates on Nanofibril Surfaces, *Biomacromolecules*, 2014, **15**(11), 4320–4325, DOI: 10.1021/bm501329v.

54 W. Li, S. Wang, W. Wang, C. Qin and M. Wu, Facile Preparation of Reactive Hydrophobic Cellulose Nanofibril Film for Reducing Water Vapor Permeability (WVP) in Packaging Applications, *Cellulose*, 2019, **26**(5), 3271–3284, DOI: 10.1007/s10570-019-02270-x.

55 K. Lee, Y. Jeon, D. Kim, G. Kwon, U.-J. Kim, C. Hong, J. W. Choung and J. You, Double-Crosslinked Cellulose Nanofiber Based Bioplastic Films for Practical Applications, *Carbohydr. Polym.*, 2021, **260**, 117817, DOI: 10.1016/j.carbpol.2021.117817.

56 J. Bras, C. Vaca-Garcia, M.-E. Borredon and W. Glasser, Oxygen and Water Vapor Permeability of Fully Substituted Long Chain Cellulose Esters (LCCE), *Cellulose*, 2007, **14**(4), 367–374, DOI: 10.1007/s10570-007-9123-2.

57 J. Wang, D. J. Gardner, N. M. Stark, D. W. Bousfield, M. Tajvidi and Z. Cai, Moisture and Oxygen Barrier Properties of Cellulose Nanomaterial-Based Films, *ACS Sustainable Chem. Eng.*, 2018, **6**(1), 49–70, DOI: 10.1021/acssuschemeng.7b03523.

58 R. R. A. Silva, C. S. Marques, T. R. Arruda, S. C. Teixeira and T. V. De Oliveira, Biodegradation, of Polymers: Stages, Measurement, Standards and Prospects, *Macromolecules*, 2023, **3**(2), 371–399, DOI: 10.3390/macromol3020023.

